New Journal and we have not received input yet 30 (2021) 100286

Contents lists available at ScienceDirect

FlatChem

journal homepage: www.sciencedirect.com/journal/flatchem

A new multifunctional two-dimensional monolayer based on silicon carbide

Nicolas F. Martins [a], Guilherme S.L. Fabris [b], Anderson R. Albuquerque [c], Julio R. Sambrano [a,*]

[a] Modeling and Molecular Simulation Group, São Paulo State University, 17033-360 Bauru, SP, Brazil
[b] Department of Materials Engineering, Federal University of Rio Grande do Norte, 59078-970 Natal, Brazil
[c] Chemistry Institute, Federal University of Rio Grande do Norte, 59078-970 Natal, Brazil

ARTICLE INFO

Keywords:
Silicon carbide
Inorganic graphenylene
DFT
Gas sensor
Battery

ABSTRACT

The family of two-dimensional materials is already a reality in the application of several technological devices. It is the motivation behind the search for unknown 2D structures using computational simulations, which can reveal the synthesis potential and their properties, thereby assisting experimentalists in targeting their applications. This is the case with the inorganic graphenylene-like silicon carbide (IGP-SiC), which is proposed and theoretically investigated in this paper for the first time. The IGP-SiC has an indirect band gap energy (3.22 eV) and thermal dynamic stability (~2100 K). Among its many applications, it has the potential to be used as an anode in next-generation batteries, as a gas sensor, and in band gap engineering in electronic devices.

1. Introduction

Silicon carbide (SiC) [1,2] can be found in a variety of crystalline forms [3], piqueing the interest of research groups in revealing new structures and properties associated with this material. Among its possible crystallographic phases, 2H-SiC is particularly appealing due to its hexagonal wurtzite structure [4], from which a one-atom thick monolayer analogous to graphene [5] can be obtained, as demonstrated by Freeman and coworkers, who predicted theoretically that wurtzite SiC and ZnO will adopt a graphitic-like structure if thinned down to a few atomic layers [6]. Moreover, this prediction was experimentally confirmed for both ZnO [7] and AlN [8] wurtzite ultrathin films.

However, the transformation of silicon carbide into a single-layer material requires the transformation of sp^3 hybridization into sp^2 hybridization, which increases the complexity of the synthesis of graphene-like silicon carbide surfaces (g-SiC) [9].

Graphenylene (GP) [10] stands out among graphene-derived structures as a monolayer with symmetrically distributed rings, a band gap of ~0.83 eV [10], and potential applications in energy storage [11–13], gas separation [14,15], and as a catalyst [16,17]. Graphenylene has recently gained attention due to its chemical synthesis via an intra- and intermolecular polymerization process [18]. Furthermore, there is a growing interest in modifying its properties through B and N atom doping, which can change its electronic, mechanical, and piezoelectric behavior [19–22], and can be extended to its other inorganic forms [23]. Nevertheless, there are inorganic structures identical to GP, such as inorganic graphenylene-like boron nitride (IGP-BN) [10,20,24], IGP-ZnO [25], and IGP-Si [26], which also have great potential for technological applications.

In this sense, by pondering over the possibility of new properties coming to light due to the combination of the special morphology of GP with the properties of SiC, we demonstrate for the first time here the existence of the inorganic graphenylene-like silicon carbide (IGP-SiC). Thus, we outline its structural, electronic, and vibrational properties while demonstrating its thermal stability to encourage experimentalists to synthesize it, as the current study based on computational modeling and simulation serves as a guide of interest.

2. Computational setup

The simulations were carried out on the CRYSTAL17 software [28] using the density functional theory (DFT) in conjunction with the B1WC [27] functional, with an all-electron basis set for all atoms. The elastic constants (C_{11}, C_{12}), Young's modulus (Y), and Poisson's ratio (ν) were calculated using the same methodology as Fabris et al. [10], while the electron density topology was analyzed according to Quantum Theory of Atoms in Molecules and Crystals (QTAIMC) [29,30]. Vibrational analysis, phonon dispersion, and cohesive energy calculations were used to confirm the structure's stability. Further details on the computational setup can be found in the Supplementary Information (SI).

* Corresponding author.
E-mail address: jr.sambrano@unesp.br (J.R. Sambrano).

https://doi.org/10.1016/j.flatc.2021.100286
Received 21 July 2021; Received in revised form 1 September 2021; Accepted 11 September 2021
Available online 16 September 2021

3. Results and discussions

IGP-SiC is planar and belongs to the P6/m space group, with lattice parameters $a = b = 8.35$ Å, containing two irreducible atoms (see the Crystallographic Information File in the SI) and has three different rings, which are classified as follows: (I) dodecahedron (C_6Si_6); (II) hexagonal (C_3Si_3), and (III) squared (C_2Si_2), as shown in Fig. 1. In comparison to GP and IGP-Si, the network parameters expand by 24.7% and contract 21.2%, respectively. Furthermore, because of the presence of carbon atoms in the network, Si-C bonds are 22.9% smaller than those seen in IGP-Si. Compared to GP, there is an expansion of 17.5% due to the high covalent bond character of the C–C bond concerning the Si-C bond. The structural stability analysis using cohesive energy reveals that the IGP-SiC is more stable than g-Si and IGP-Si, as shown in the SI.

Fig. 1 depicts the results of the simulations regarding the mechanical properties and band gap energy, revealing that IGP-SiC is ~2.2 times more susceptible to deformations than GP. It is also 3 times more rigid than IGP-Si, possibly due to the planarity and configuration of Si-C bonds. Except for IGP-Si, IGP-SiC has a higher Poisson's ratio (ν) than all other related materials, indicating that its structure is more deformable in the transverse direction.

Fig. 2 depicts the band structure, density of states, and electron density of IGP-SiC, which helps in the understanding of its electronic behavior. The simulation results for g-SiC are also shown for comparison.

IGP-SiC has an indirect band gap energy (E_{gap}) of 3.22 eV (Fig. 2A), with apparent flat bands between the region of the M and K points in the top and bottom of valence bands (VB) and conduction bands (CB), respectively, which indicates an increase in electron effective mass and a decrease in electronic mobility, a behavior similar to that of GP.

Unlike graphene and g-Si, which have zero E_{gap}, g-SiC has an E_{gap} of 3.65 eV at the ~K point, which is slightly higher than IGP-SiC, as shown in Fig. 2. Such a reduction in the band gap can be attributed to a significant structural and orbital superposition change in the formation of IGP-SiC. The density of states reveals that the edge of the VB of IGP-SiC has a substantial contribution from both Si and C atoms, and a very small contribution from C atoms in CB, which differs from the inverse behavior observed for g-SiC.

The analysis of the Laplacian and the gradient of the electron density at the bond critical points (BCP) (see Fig. 2) provides relevant information on the trajectory of charge density and aids in understanding the behavior of chemical bonds in this new structure, where the blue dotted lines represent charge depletion and the red lines represent charge accumulation, respectively. For IGP-SiC, it can be observed that the gradients intersect in the center of the rings; however, it was discovered that the density is located near the border of the dodecahedron, which can facilitate the diffusion of atoms or small molecules. On the other hand, high density is found in rings II and III (Fig. 1). In the case of g-SiC, charge accumulation in the Si atom directs the electron transfer toward C, which is more negative. Table S2 contains a comparison of the results of other two-dimensional materials, as well as additional comments.

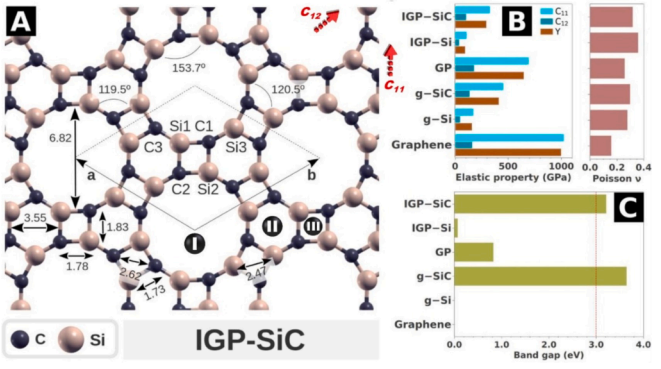

Fig. 1. (A) IGP-SiC unit cell with bond length (Å) and bond angles (°). (B) Elastic constants (GPa) and Poisson's ratio (ν), and (C) band gap energy of IGP-SiC and related materials. I, II, and III represent the dodecahedral, hexagonal, and squared rings, respectively.

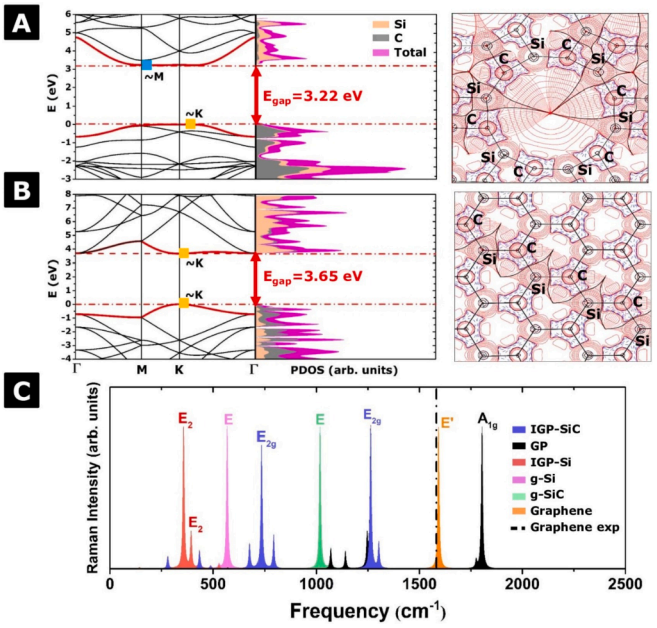

Fig. 2. Band structure, density of states, Laplacian of the electron density (blue dashed lines), and trajectory of charge density (red lines) of (A) IGP-SiC, (B) g-SiC, and (C) Raman vibrational spectrum of IGP-SiC, GP [10], IGP-Si [26], g-Si [26], g-SiC, graphene [10] and the experimental graphene [31].

The simulations show that there are no imaginary frequencies in the phonon calculation, signaling the dynamic stability of IGP-SiC, as shown in Table S3. Furthermore, it is demonstrated that IGP-SiC is thermally stable, as the structure remains intact up to 2100 K, and starts to break at ~2180 K, whereas g-SiC supports more than 3000 K, as shown in our simulation, due to the similar morphology to graphene. The video of thermal stability and details about the simulation can be found in the SI.

To determine the fingerprint of IGP-SiC (Fig. 2C), the Raman spectrum was analyzed, as well as the spectrum of GP, IGP-Si, g-Si, and g-SiC. By doing so, it was possible to identify that IGP-SiC has 10 active modes, $\Gamma = 4E_{2g} + 4A_g + 2E_{1g}$, with the most intense at 733.9 cm^{-1} (E_{2g}) and 1263.4 cm^{-1} (E_{2g}), while IGP-Si [26] has active modes at 357.6 cm^{-1} (E_2) and 394.1 cm^{-1} (E_2), and GP [10] has 8 active modes, with the most intense at 1743.5 cm^{-1} (A_{1g}). Contrariwise, g-SiC and g-Si [26] have a single active Raman mode at 1017.7 cm^{-1} (E) and 555.5 cm^{-1} (E), respectively. For comparison purposes, the experimental G-band of graphene obtained by Dresselhaus et al. [31] and our theoretical estimate were added. This result demonstrates that the g-SiC peak is nearly the average of the g-Si (E) and graphene (E') peaks. The accuracy of our graphene theoretical results provides us with a high degree of reliability for the predicted data based on our methodology.

To exemplify one of the potential applications of this new material, the energy barrier (E_{bar}) for the diffusion of alkaline metals and noble gases at ring I (Fig. 3) was calculated, as well as the height barrier ($|r_0|$) with correction for the basis set superposition error (BSSE) and Bader charges (Q), the values of which can be found in the SI.

Fig. 3 shows that there is a spontaneous diffusion of the Na atom in ring I, as well as a small (very low) energy barrier for the Li (~0.18 eV) and K (11 meV) atoms. This behavior indicates a preference for diffusion in the central ring, allowing the design of an anode composed of IGP-SiC layers, where atom diffusion between layers can be guaranteed, thereby favoring the process of electric charge and discharge. Furthermore, the presence of metal atoms in the IGP-SiC semiconductor monolayer

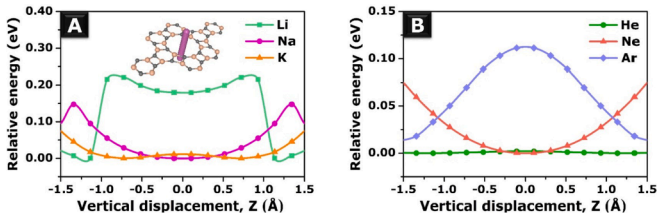

Fig. 3. Vertical displacement and energy profile of (A) Li, Na and K atoms, and (B) He, Ne and Ar atoms, across ring I by restricted region between −1.5 Å and 1.5 Å.

imparts a conductive character to the material, implying that this structure could be used as an anode in next-generation batteries as well as in other technological applications. The energy barriers were also investigated in the case of noble gas diffusion (Fig. 3B). The He atom exhibits almost spontaneous diffusion with a very low barrier energy (2 meV), while the Ar atom exhibits a small barrier energy (0.11 eV). Additionally, the Ne atoms can be trapped in the center of the dodecahedral pore, demonstrating that the IGP-SiC can function as a porous membrane in the noble gases separation. More information can be found in the SI.

IGP-SiC can also be transformed as a magnetic and catalytic material with multiple functionalities, as shown in Fig. 4.

The incorporation of transition metal atoms on IGP-SiC (for example, replacing two Si atoms with two Fe atoms) can trigger modulable magnetic properties. Fig. 4 depicts the Fe-doped IGP-SiC in ferromagnetic solution as a possibility to modulate the electronic configuration of IGP-SiC, lowering its band gap energy to 1.52 eV. (Fig. 4A). Another area for future research is gas adsorption, such as nitrogen monoxide NO, which is characterized by physisorption ($E_{ads} = -8.76$ kcal/mol) with a low change in the band gap (Fig. 4B).

The adsorption of NO on Fe-doped IGP-SiC was carried out to test the effect of the transition metal on the interacting system (Fig. 4C). The adsorption on the Fe site was most favorable ($E_{ads} = -58.11$ kcal/mol), with a significant band gap decrease ($E_{gap} = 0.87$ eV), allowing the use of Fe-doped IGP-SiC as a potential selective toxic gas sensor. The influence of magnetic states in NO adsorption/desorption behavior requires further investigation; this is an insight that could lead to new theoretical and experimental studies. More details about the configurations can be found in the SI.

Conclusions

Because it has a planar structure with symmetrically distributed rings, IGP-SiC is more resistant than IGP-Si. It also has high thermal and dynamic stability, withstanding temperatures above ~2100 K, which indicates its broad synthesis potential. The presence of a low charge density in ring I confirms its barrier energy, which is favorable to the diffusion of atoms and small molecules in this ring, as IGP-SiC begins to have a conductive character from interactions with Li, Na, and K, demonstrating its applicability in energy-generating devices. Furthermore, IGP-SiC is presented as a promising porous membrane for noble gas separation, as evidenced by the diffusion process of He, Ne and Ar in the central ring.

Finally, initial studies of Fe-doped IGP-SiC in ferromagnetic solution indicate a change in the surface electronic configuration, demonstrating that doping with a transition metal can reveal a magnetic material. As a result of its interaction with NO, the Fe-doped IGP-SiC can also be a potentially toxic gas sensor.

CRediT authorship contribution statement

Nicolas F. Martins: Conceptualization, Methodology, Software, Validation, Formal analysis, Writing – original draft, Writing – review & editing. **Guilherme S.L. Fabris:** Conceptualization, Methodology, Software, Validation, Formal analysis, Writing – original draft, Writing – review & editing. **Anderson R. Albuquerque:** Conceptualization, Methodology, Software, Validation, Formal analysis, Writing – original draft, Writing – review & editing. **Julio R. Sambrano:** Conceptualization, Funding acquisition, Investigation, Methodology, Project administration, Resources, Software, Supervision, Validation, Visualization, Writing – original draft, Writing – review & editing.

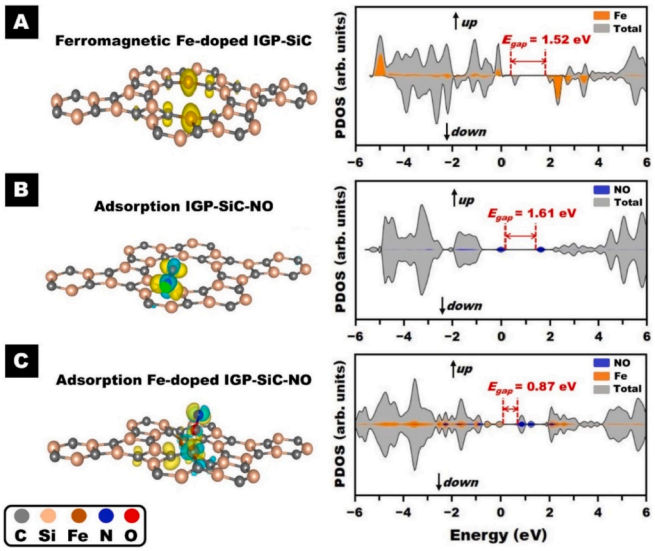

Fig. 4. (Left) Side view of the structure with spin density isosurfaces and (right) the projected density os states of (A) Ferromagnetic Fe-doped IGP-SiC, (B) Adsorption IGP-SiC-NO and (C) Adsorption Fe-doped IGP-SiC-NO. Isosurfaces (0.005 e/Å^3) in yellow and blue denote α and β spin densities, respectively.

Declaration of Competing Interest

The authors declare that they have no known competing financial interests or personal relationships that could have appeared to influence the work reported in this paper.

Acknowledgments

This work was supported by the Brazilian funding agencies FAPESP (2019/08928-9, 2013/07296-2, 2020/10380-9), CAPES – Finance Code 001 – (88887.467334/2019-00) and CNPq Universal program (grant no. 420062/2016-5). The computational facilities were supported by resources supplied by the Molecular Simulations Laboratory (São Paulo State University, Bauru, Brazil) and High-Performance Computing Center (NPAD) at UFRN.

Appendix A. Supplementary data

Supplementary data to this article can be found online at https://doi.org/10.1016/j.flatc.2021.100286.

References

[1] X.u. She, A.Q. Huang, O. Lucia, B. Ozpineci, Review of silicon carbide power devices and their applications, IEEE Trans. Ind. Electron. 64 (10) (2017) 8193–8205, https://doi.org/10.1109/TIE.2017.2652401.
[2] C.I. Harris, S. Savage, A. Konstantinov, M. Bakowski, P. Ericsson, Progress towards SiC products, Appl. Surf. Sci. 184 (1-4) (2001) 393–398, https://doi.org/10.1016/S0169-4332(01)00525-6.
[3] A.L. Ortiz, F. Sánchez-Bajo, F.L. Cumbrera, F. Guiberteau, The prolific polytypism of silicon carbide, J. Appl. Crystallogr. 46 (1) (2013) 242–247, https://doi.org/10.1107/S0021889812049151.

[4] L. Patrick, D.R. Hamilton, W.J. Choyke, Growth, luminescence, selection rules, and lattice sums of SiC with Wurtzite structure, Phys. Rev. 143 (2) (1966) 526–536, https://doi.org/10.1103/PhysRev.143.526.
[5] A.K. Geim, K.S. Novoselov, The rise of graphene, Nat. Mater. 6 (3) (2007) 183–191, https://doi.org/10.1038/nmat1849.
[6] C.L. Freeman, F. Claeyssens, N.L. Allan, J.H. Harding, Graphitic nanofilms as precursors to Wurtzite films: theory, Phys. Rev. Lett. 96 (2006), 066102, https://doi.org/10.1103/PhysRevLett.96.066102.
[7] C. Tusche, H.L. Meyerheim, J. Kirschner, Observation of depolarized ZnO(0001) monolayers: formation of unreconstructed planar sheets, Phys. Rev. Lett. 99 (2007), 026102, https://doi.org/10.1103/PhysRevLett.99.026102.
[8] P. Tsipas, S. Kassavetis, D. Tsoutsou, E. Xenogiannopoulou, E. Golias, S.A. Giamini, C. Grazianetti, D. Chiappe, A. Molle, M. Fanciulli, A. Dimoulas, Evidence for graphite-like hexagonal AlN nanosheets epitaxially grown on single crystal Ag (111), Appl. Phys. Lett. 103 (25) (2013) 251605, https://doi.org/10.1063/1.4851239.
[9] S. Chabi, K. Kadel, Two-dimensional silicon carbide: emerging direct band gap semiconductor, Nanomaterials 10 (2020) 2226, https://doi.org/10.3390/nano10112226.
[10] G.S.L. Fabris, N.L. Marana, E. Longo, J.R. Sambrano, Theoretical study of porous surfaces derived from graphene and boron nitride, J. Solid State Chem. 258 (2018) 247–255, https://doi.org/10.1016/j.jssc.2017.10.025.
[11] M. Hankel, D.J. Searles, Lithium storage on carbon nitride, graphenylene and inorganic graphenylene, Phys. Chem. Chem. Phys. 18 (21) (2016) 14205–14215, https://doi.org/10.1039/C5CP07356A.
[12] Y. Bahari, B. Mortazavi, A. Rajabpour, X. Zhuang, T. Rabczuk, Application of two-dimensional materials as anodes for rechargeable metal-ion batteries: a comprehensive perspective from density functional theory simulations, Energy Storage Mater. 35 (2021) 203–282, https://doi.org/10.1016/j.ensm.2020.11.004.
[13] G. da Silva Lopes Fabris, A. dos Reis Albuquerque, R. Dovesi, J. Ricardo Sambrano, A promising carbon-based nanosheet as a suitable Na-anode material, Mater. Sci. Eng. B Solid-State Mater. Adv. Technol. 268 (2021) 115121, https://doi.org/10.1016/j.mseb.2021.115121.
[14] P. Rezaee, H.R. Naeij, Graphenylene–1 membrane: an excellent candidate for hydrogen purification and helium separation, Carbon N. Y. 157 (2020) 779–787, https://doi.org/10.1016/j.carbon.2019.10.064.
[15] L. Wang, F. Li, J. Wang, Y. Li, W. Li, Y. Yang, M. Zhao, Y. Qu, High-efficiency helium separation through an inorganic graphenylene membrane: a theoretical study, Phys. Chem. Chem. Phys. 22 (17) (2020) 9789–9795, https://doi.org/10.1039/D0CP00154F.
[16] Y. Tang, W. Chen, Z. Wang, G. Zhao, Y. Cui, Z. Li, Y. Li, Z. Feng, X. Dai, Formation, electronic, gas sensing and catalytic characteristics of graphene-like materials: a first-principles study, Appl. Surf. Sci. 530 (2020) 147178, https://doi.org/10.1016/j.apsusc.2020.147178.
[17] W. Chen, Z. Wang, Y. Cui, Z. Li, Y. Li, X. Dai, Y. Tang, Graphenylene-supported single-atom (Ru and Mo) catalysts for CO and NO oxidations, New J. Chem. 44 (36) (2020) 15733–15741, https://doi.org/10.1039/D0NJ03842C.
[18] Q.-S. Du, P.-D. Tang, H.-L. Huang, F.-L. Du, K. Huang, N.-Z. Xie, S.-Y. Long, Y.-M. Li, J.-S. Qiu, R.-B. Huang, A new type of two-dimensional carbon crystal prepared from 1,3,5-trihydroxybenzene, Sci. Rep. 7 (2017) 40796, https://doi.org/10.1038/srep40796.
[19] A. Freitas, L.D. Machado, C.G. Bezerra, R.M. Tromer, L.F.C. Pereira, S. Azevedo, B x C y N z hybrid graphenylene: stability and electronic properties, RSC Adv. 8 (44) (2018) 24847–24856, https://doi.org/10.1039/C8RA02188K.
[20] J. Xu, S. Zhou, P. Sang, J. Li, L. Zhao, Inorganic graphenylene as a promising novel boron nitrogen membrane for hydrogen purification: a computational study, J. Mater. Sci. 52 (17) (2017) 10285–10293, https://doi.org/10.1007/s10853-017-1246-8.
[21] L. Villegas-Lelovsky, R. Paupitz, Graphenylene-based nanoribbons for novel molecular electronic devices, Phys. Chem. Chem. Phys. 22 (48) (2020) 28365–28375, https://doi.org/10.1039/D0CP04188B.
[22] G.S.L. Fabris, N.L. Marana, E. Longo, J.R. Sambrano, Piezoelectric response of porous nanotubes derived from hexagonal boron nitride under strain influence, ACS Omega 3 (10) (2018) 13413–13421, https://doi.org/10.1021/acsomega.8b0163410.1021/acsomega.8b01634.s001.
[23] G.S.L. Fabris, C.A. Paskocimas, J.R. Sambrano, R. Paupitz, One- and two-dimensional structures based on gallium nitride, J. Solid State Chem. 303 (2021) 122513, https://doi.org/10.1016/j.jssc.2021.122513.
[24] E. Perim, R. Paupitz, P.A.S. Autreto, D.S. Galvao, Inorganic graphenylene: a porous two-dimensional material with tunable band gap, J. Phys. Chem. C 118 (41) (2014) 23670–23674, https://doi.org/10.1021/jp502119y.
[25] G.S.L. Fabris, N.L. Marana, José.A.S. Laranjeira, E. Longo, J.R. Sambrano, New two-dimensional zinc oxide nanosheets: properties, stability, and interconversion, Mater. Lett. 275 (2020) 128067, https://doi.org/10.1016/j.matlet.2020.128067.
[26] G.S.L. Fabris, N.L. Marana, E. Longo, J.R. Sambrano, Porous silicene and silicon graphenylene-like surfaces: a DFT study, Theor. Chem. Acc. 137 (1) (2018), https://doi.org/10.1007/s00214-017-2188-6.
[27] D.I. Bilc, R. Orlando, R. Shaltaf, G.M. Rignanese, J. Íñiguez, P. Ghosez, Hybrid exchange-correlation functional for accurate prediction of the electronic and structural properties of ferroelectric oxides, Phys. Rev. B - Condens. Matter Mater. Phys. 77 (2008) 1–13, https://doi.org/10.1103/PhysRevB.77.165107.
[28] R. Dovesi, A. Erba, R. Orlando, C.M. Zicovich-Wilson, B. Civalleri, L. Maschio, M. Rérat, S. Casassa, J. Baima, S. Salustro, B. Kirtman, Quantum-mechanical condensed matter simulations with CRYSTAL, Wiley Interdiscip. Rev. Comput. Mol. Sci. 8 (2018) 1–36, https://doi.org/10.1002/wcms.1360.
[29] R.F.W. Bader, Atoms in Molecules: a quantum theory (International Series of Monographs on Chemistry), Oxford University Press, 1994.
[30] C. Gatti, S. Casassa, User's Manual, (2017).
[31] M.S. Dresselhaus, A. Jorio, M. Hofmann, G. Dresselhaus, R. Saito, Perspectives on carbon nanotubes and graphene raman spectroscopy, Nano Lett. 10 (3) (2010) 751–758, https://doi.org/10.1021/nl904286r.